Calculation of Redox Potentials and pK_a Values of Hydrated Transition Metal Cations by a Combined Density Functional and Continuum Dielectric Theory

Jian Li,* Cindy L. Fisher, Jun L. Chen, Donald Bashford, and Louis Noodleman*

Department of Molecular Biology, MB 1, The Scripps Research Institute, La Jolla, California 92037

Received November 2, 1995[⊗]

Density functional and continuum dielectric theories have been combined to calculate molecular properties such as hydration enthalpies, redox potentials, and absolute pK_a values of transition metal cations in solution. The discrete cluster model, which is treated explicitly by density functional theory, includes six waters in the first hydration shell and another twelve waters in the second shell. The solvent reaction field is obtained from a finite-difference solution to the Poisson−Boltzmann equation and is coupled to the nonlocal density functional calculation in a self-consistent way. The calculated hydration enthalpies are 409, 1073, 431, and 1046 kcal/mol for Mn^{2+}, Mn^{3+}, Fe^{2+}, and Fe^{3+}, respectively, comparing fairly well to the experimental measurements of 440, 1087, 465, and 1060 kcal/mol. The calculated redox potentials for the Mn^{2+}/Mn^{3+} and Fe^{2+}/Fe^{3+} pairs are 1.59 and 1.06 V, respectively, in good agreement with the experimental values of 1.56 and 0.77 V. The computed absolute pK_a values, 14.0, −6.5, 9.0, and −4.0 for Mn^{2+}, Mn^{3+}, Fe^{2+}, and Fe^{3+}, respectively, deviate significantly from the experimental results of 10.6, 0.1, 9.5, and 2.2 but show the proper behavior with changes in oxidation state and metal type. The calculated redox potentials and pK_a values appear to converge toward the experimental data with increasing size of the cluster models. For such highly charged cations, the second hydration shell in the cluster model is indispensable, since this buffer shell retains strong hydrogen bonds and electron transfer between the inner and outer shells as well as the solute−solvent dispersion interaction.

Introduction

Condensed phase environments impose significant effects on the properties and reactivities of molecules. Often the quantum chemical picture of a molecule *in vacuo* is insufficient for describing the electronic structures and reactions of molecules in solution and of active sites in proteins.[1] The last decade has witnessed an upsurge of theoretical methods that incorporate solvent effects into quantum mechanical calculations. As a common strategy, these methods treat the solute molecule quantum mechanically while handling the solvent classically. For instance, many methods like the combined QM/MM approach consider the microscopic structure of solvent molecules explicitly. The energy of the solvent molecules is averaged by molecular dynamics, the Monte Carlo approach, or force field based minimization, and the periodic boundary conditions or spherical boundary conditions are adopted to deal with the infinite solvent environment.[2] Another class of methods employs a dielectric continuum model or polarizable dipoles to represent the entire solvent region.[3] In the continuum model, the solute molecule is placed in a cavity immersed in the solvent continuum and the solvent reaction field exerting on the solute is then taken into account in a self-consistent way. This self-consistent reaction field approach has been implemented at all levels of quantum mechanics including semiempirical,[4] ab initio,[5] and density functional methods.[6] The application of this approach to neutral and charged organic molecules is very promising, but few calculations have been reported on transition metal species.

Our main interests focus on metalloproteins and metalloenzymes in which the active sites contain charged high-spin metal

[⊗] Abstract published in *Advance ACS Abstracts,* July 15, 1996.

(1) (a) Warshel, A. *Computer Modelling of Chemical Reactions in Enzymes and Solutions;* Wiley: New York, 1991. (b) van Gunsteren, W. F.; Luque, F. J.; Timms, D.; Torda, A. E. *Annu. Rev. Biophys. Biomol. Struct.* **1994,** *23*, 847. (c) Cramer, C. J.; Truhlar, D. G. *Structure and Reactivity in Aqueous Solution: Characterization of Chemical and Biological Systems*; ACS Symposium Series 568; American Chemical Society: Washington, DC, 1994. (d) Honig, B.; Sharp, K.; Yang, A.-S. *J. Phys. Chem.* **1993**, *97*, 1101. (e) Smith, P. E.; Pettitt, B. M. *J. Phys. Chem.* **1994,** *98*, 9700. (f) Kollman, P. *Chem. Rev.* **1993**, *93*, 2395.

(2) (a) Jorgensen, W. L. *Acc. Chem. Res.* **1989**, *22*, 184. (b) Jorgensen, W. L.; Buckner, J. K. *J. Phys. Chem.* **1987**, *91*, 6038. (c) Gao, J.; Xia, X. *Science* **1992**, *258*, 631. (d) Gao, J. *J. Am. Chem. Soc.* **1994,** *116*, 9324. (e) Bash, P.; Field, M.; Karplus, M. *J. Am. Chem. Soc.* **1987**, *109*, 8092. (f) Floris, F.; Persico, M.; Tani, A.; Tomasi, J. *Chem. Phys. Lett.* **1992**, *199*, 518. (g) Laasonen, K.; Klein, M. L. *J. Am. Chem. Soc.* **1994**, *116*, 11620. (h) Zeng, J.; Craw, J. S.; Hush, N. S.; Reimers, J. R. *J. Chem. Phys.* **1993,** *99*, 1482. (i) Warshel, A. *J. Phys. Chem.* **1979**, *83*, 1640. (j) Luzhkov, V.; Warshel, A. *J. Comput. Chem.* **1992**, *13*, 199.

(3) (a) Tapia, O. In *Quantum Theory of Chemical Reactions;* Daudel, R., Pullman, A., Salam, L., Veillard, A., Eds.; Riedel: Dordrecht, The Netherlands, 1980; Vol. II. (b) Tomasi, J.; Bonaccorsi, R.; Cammi, R.; Olivares del Valle, F. J. *J. Mol. Struct. (THEOCHEM)* **1991**, *234*, 401. (c) Warshel, A.; Russell, S. T. *Q. Rev. Biophys.* **1984**, *17*, 283.

(4) (a) Cramer, C. J.; Truhlar, D. G. In *Reviews in Computational Chemistry;* Lipkowitz, K. B., Boyd, D. B., Eds.; VCH Publishers: Weinheim, Germany, 1995; Vol. 6. (b) Cramer, C. J.; Truhlar, D. G. *J. Am. Chem. Soc*. **1991**, *113*, 8305. (c) Cramer, C. J.; Truhlar, D. G. *Science* **1992**, *256*, 213. (d) Liotard, D. A.; Hawkins, G. D.; Lynch, G. C.; Cramer, C. J.; Truhlar, D. G. *J. Comput. Chem.* **1995**, *16*, 422. (e) Karelson, M. M.; Zerner, M. C. *J. Phys. Chem.* **1992,** *96*, 6949. (f) Furuki, T.; Sakurai, M.; Inoue, Y. *J. Comput. Chem.* **1995**, *16*, 378. (g) Wang, B.; Ford, G. P. *J. Chem. Phys.* **1992**, *97*, 4162.

(5) (a) Tomasi, J.; Persico, M. *Chem. Rev.* **1994,** *94*, 2027. (b) Miertus, S.; Scrocco, E.; Tomasi, J. *Chem. Phys*. **1981**, *55*, 117. (c) Wong, M. W.; Frisch, M. J.; Wiberg, K. B. *J. Am. Chem. Soc*. **1991**, *113*, 4776. (d) Marcos, E. S.; Pappalardo, R. R.; Rinaldi, D. *J. Phys. Chem*. **1991**, *95*, 8928. (e) Tannor, D. J.; Marten, B.; Murphy, R.; Friesner, R. A.; Sitkoff, D.; Nicholls, A.; Ringbalda, M.; Goddard, W. A., III; Honig, B. *J. Am. Chem. Soc.* **1994**, *116*, 11875. (f) Truong, T. N.; Stefanovich, E. V. *Chem. Phys. Lett.* **1995**, *240*, 257.

(6) (a) Chen, J. L.; Noodleman, L.; Case, D. A.; Bashford, D. *J. Phys. Chem.* **1994**, *98*, 11059. (b) Richardson, W. H.; Peng, C. Y.; Bashford, D.; Noodleman, L.; Case, D. A. *Int. J. Quant. Chem*. **1996**, in press. (c) Ruiz-Lopez, M. F.; Bohr, F.; Martins-Costa, M. T. C.; Rinaldi, D. *Chem. Phys. Lett.* **1994**, *221*, 109. (d) Adamo, C.; Lelj, F. *Chem. Phys. Lett.* **1994**, *223*, 54. (e) Fortunelli, A.; Tomasi, J. *Chem. Phys. Lett.* **1994**, *231*, 34. (f) Baldridge, K.; Fine, R.; Hagler, A. *J. Comput. Chem.* **1994**, *15*, 1217. (g) Hall, R. J.; Davidson, M. M.; Burton, N. A.; Hillier, I. H. *J. Phys. Chem*. **1995**, *99*, 921.

S0020-1669(95)01428-5 CCC: $12.00

centers.[7] For such systems, both environmental effects from the protein and intrinsic difficulties arising from the transition metal sites represent challenges to theoretical calculations. Density functional theory has proven an effective method for the study of transition metal complexes.[8] The recent implementation combining density functional and continuum dielectric theories[6a] equips us with more appropriate tools. In this combined method, the electronic structure of the solute is computed by density functional methods in the presence of a solution reaction field. The reaction field is then evaluated from a finite-difference solution to the Poisson−Boltzmann equation, and self-consistency between the reaction field potential and the electronic structure is achieved by iteration. This technique has been applied to study active site models of several metalloenzymes including the iron−sulfur clusters (non-self-consistent)[9] and superoxide dismutase (SOD)[10] in high dielectric solvent. The extension of this method to investigate the active sites including protein and protein−solvent environments is currently underway.

In this paper, we use the combined density functional and continuum dielectric techniques to calculate redox potentials and pK_a values for hydrated metal cations. These properties are closely related to the energetics of electron and proton transfer in inorganic and related bioinorganic systems. Calculation of these properties requires not only a high-level quantum mechanical evaluation of the ionization potential and proton affinity in gas phase but also a precise accounting of solvation energy. In addition to the electrostatic interaction between the solute and solvent, highly charged cations also induce charge transfer between the metal center and surrounding aqueous environment, which in turn affects the hydrogen bonds within the hydration shells. To this end, building a reasonable cluster model that retains most of the quantum effects within the solute interior is vital. The goal of this study is therefore twofold. First, we want to validate the usefulness of the current method for calculations on transition metal systems, especially for properties like redox potentials and pK_a values. Second, by constructing supermolecular models with different numbers of hydration shells, we want to explore to what extent the environment in the quantum region of the combined discrete−continuum model should be explicitly included. The same question applies when using these methods to study metalloproteins and metalloenzymes: How big should the active site be?

Computational Details and Cluster Models

1. Density Functional Calculations. All calculations were carried out using the Amsterdam Density Functional (ADF) package and its precursor version AMOL[11] with modifications to include a self-consistent reaction field.[6a] The local density approximation (LDA) for exchange and correlation used the parametrization of Vosko, Wilk, and Nusair.[12] The nonlocal corrections (NL), which are based on Becke's gradient correction to exchange[13] and Perdew's correction to correlation,[14] were added in each self-consistent cycle. Convergence was achieved once the change in the mean of diagonal elements of the density matrix was smaller than 0.0001. The numerical integration scheme adopted was the polyhedron method developed by te Velde *et al.*[15] with the accuracy parameter ACCINT of 4.0. A set of uncontracted triple-ζ Slater-type orbitals (STO)[16] was employed for the $(n + 1)$s, $(n + 1)$p, and *n*d valence orbitals of the transition metal atoms. For the 2s and 2p orbitals of oxygen and 1s orbital of hydrogen, use was made of the same quality basis augmented by extra d and p functions, respectively. The inner core shells were treated by the frozen core approximation. A set of auxiliary s, p, d, f, and g STO functions, centered on all nuclei, was introduced to fit the molecular density and to represent Coulomb and exchange potentials accurately.[17] All calculations were done with a spin-unrestricted scheme.

Geometry optimization of cluster models was done according to the analytic gradient method implemented at the LDA level by Versluis *et al.* and at the NL level by Fan *et al.*[18] The optimization used the Newton−Raphson method, and the hessian was updated with the Broyden−Fletcher−Goldfarb−Shanno strategy.[19] Convergence was achieved when changes in coordinate values were less than 0.005 Å and the norm of all gradient vectors was smaller than 0.01. Frequencies of some species were evaluated from force constants calculated by numerical differentiation of energy gradients.[20] The relativistic correction was estimated by a quasi-relativistic calculation that included the mass−velocity and Darwin terms in the first-order Hamiltonian and the induced density changes.[21] In this scheme, the core orbitals were replaced by the relativistic ones which were obtained by numerical solution of the atomic Dirac equation.

2. Fitting of ESP Charges. A modified version of the CHELPG code of Breneman and Wiberg[22] was used to fit the point charges from the molecular electrostatic potentials (ESP) calculated by the ADF code. The total net charge of the molecule and the three Cartesian dipole moment components from density functional calculations were adopted as constraint conditions for the fit.[6a] The fitted points lay on a cubic grid between the van der Waals radius and the outer atomic radius with a grid spacing of 0.2 Å. The outer atomic radius for all atoms used was 5.0 Å, and the van der Waals radii for $Mn^{2+/3+}$, $Fe^{2+/3+}$, O, and H were 1.5, 1.5, 1.4, and 1.2 Å, respectively. In order to minimize the uncertainties in the fitting procedure, the singular value decomposition (SVD)[23] method was introduced into the code to obtain a model with stable atomic charges and an accurate molecular dipole moment.[9]

3. Solution of the Poisson Equation and Solvation Energy. The MEAD (Macroscopic Electrostatics with Atomic Detail) program suite developed by Bashford,[24] which solves the Poisson−Boltzmann equation by a numerical finite-difference method, was employed to calculate the solvent reaction field potential induced by the atomic ESP charges

(7) Frausto da Silva, J. J. R.; Williams, R. J. P. *The Biological Chemistry of the Elements*; Clarendon: Oxford, U.K., 1991.
(8) Ziegler, T. *Chem. Rev.* **1991**, *91*, 651.
(9) Mouesca, J.-M.; Chen, J. L.; Noodleman, L.; Bashford, D.; Case, D. A. *J. Am. Chem. Soc.* **1994**, *116*, 11898.
(10) Fisher, C. L.; Chen, J. L.; Li, J.; Bashford, D.; Noodleman, L. *J. Phys. Chem.*, in press.
(11) (a) Baerends, E. J.; Ellis, D. E.; Ros, P. *Chem. Phys*. **1973**, *2*, 41. (b) Ravenek, W. In *Algorithms and Applications on Vector and Parallel Computes*; te Riele, H. J. J., Dekker, Th. J., van de Vorst, H. A., Eds.; Elsevier: Amsterdam, 1987.
(12) Vosko, S. H.; Wilk, L.; Nusair, M. *Can. J. Phys*. **1980**, *58*, 1200.
(13) Becke, A. D. *J. Chem. Phys*. **1986,** *84*, 4524.
(14) Perdew, J. P. *Phys. Rev. B* **1986**, *33*, 8822; **1986**, *34*, 7406 (erratum).
(15) (a) Boerrigter, P. M.; te Velde, G.; Baerends, E. J. *Int. J. Quant. Chem*. **1988**, *33*, 87. (b) te Velde, G.; Baerends, E. J. *J. Comput. Phys.* **1992,** *99*, 84.
(16) (a) Snijders, J. G.; Baerends, E. J.; Vernooijs, P. *At. Nucl. Data Tables* **1982**, *26*, 483. (b) Vernooijs, P.; Snijders, J. G.; Baerends, E. J. *Slater Type Basis Functions for the Whole Periodic System;* Internal Report; Free University of Amsterdam: Amsterdam, The Netherlands, 1981.
(17) Krijn, J.; Baerends, E. J. *Fit Functions in the HFS-method;* Internal Report (in Dutch); Free University of Amsterdam: Amsterdam, The Netherlands, 1984.
(18) (a) Versluis, L.; Ziegler, T. *J. Chem. Phys.* **1988,** *88*, 322. (b) Fan, L.; Ziegler, T. *J. Chem. Phys.* **1991,** *95*, 7401.
(19) (a) Schlegel, H. B. In *Ab initio Methods in Quantum Chemistry-I*; Lawley, K. P., Ed.; *Adv. Chem. Phys. Vol. 67*; Wiley: New York, 1987. (b) Head, J. D.; Zerner, M. C. *Adv. Quantum Chem*. **1988**, *20*, 1.
(20) (a) Fan, L.; Versluis, L.; Ziegler, T.; Baerends, E. J.; Ravenek, W. *Int. J. Quantum Chem*. **1988,** *Symp 22*, 173. (b) Fan, L.; Ziegler, T. *J. Chem. Phys.* **1991**, *94*, 6057.
(21) (a) Ziegler, T.; Tschinke, V.; Baerends, E. J.; Snijders, J. G.; Ravenek, W. *J. Phys. Chem*. **1989**, *93*, 3050. (b) Snijders, J. G.; Baerends, E. J. *Mol. Phys*. **1979**, *36*, 1789. (c) Snijders, J. G.; Baerends, E. J.; Ros, P. *Mol. Phys*. **1979**, *38*, 1909.
(22) Breneman, C. M.; Wiberg, K. B. *J. Comput. Chem.* **1990**, *11*, 361.
(23) Press, W. H.; Flanery, B. P.; Teukolsky, S. A.; Vetterling, W. T. *Numerical Recipes, The Art of Scientific Computing;* Cambridge University Press: Cambridge, U.K., 1986.
(24) (a) Bashford, D. *Curr. Op. Struct. Biol.* **1991,** *1*, 175. (b) Bashford, D.; Gerwert, K. *J. Mol. Biol.* **1992,** *224*, 473. (c) Lim, C,; Bashford, D.; Karplus, M. *J. Phys. Chem.* **1991**, *95*, 5610. (d) Bashford, D.; Case, D. A.; Dalvit, C.; Tennant, L.; Wright, P. E. *Biochemistry* **1993**, *32*, 8045.

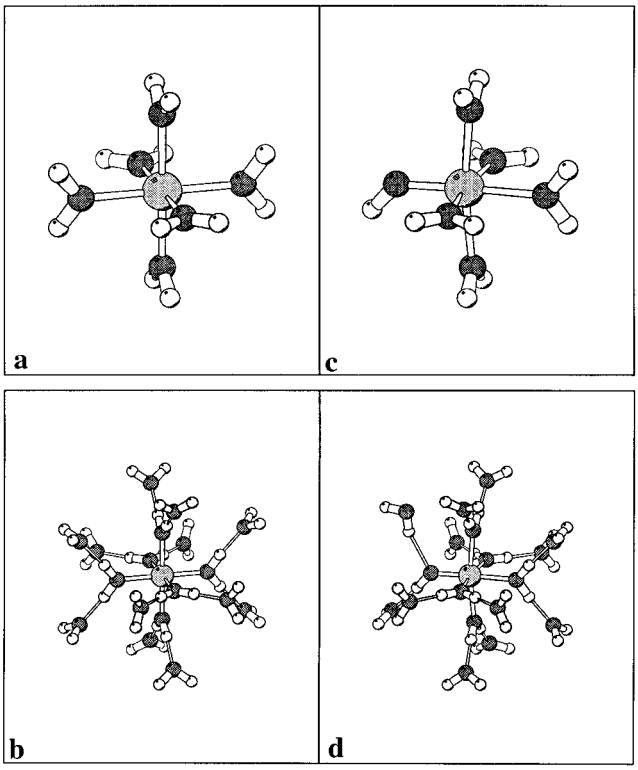

Figure 1. Structures of the discrete cluster models: (a) $[M(H_2O)_6]^{m+}$; (b) $[M(H_2O)_{18}]^{m+}$; (c) $[M(OH)(H_2O)_5]^{(m-1)+}$; (d) $[M(OH)(H_2O)_{17}]^{(m-1)+}$. This figure was prepared using MOLSCRIPT: Kraulis, P. J. *J. Appl. Crystallogr.* **1991**, *24*, 946.

of the solute molecule. For this purpose, the solute molecule within an interior region was assigned a dielectric constant of $\epsilon_i = 1$, while the region outside was assigned the experimental solvent dielectric of $\epsilon_o = 80$ representing aqueous solution. For the purpose of defining the dielectric boundary, atomic radii of 1.55 Å ($Mn^{2+/3+}$ and $Fe^{2+/3+}$), 1.40 Å (O), and 1.20 Å (H) were chosen. The solute interior was defined as the region inaccessible to any part of a probe sphere of radius 1.4 Å rolling on the molecular surface of the atomic spheres. The boundary between the interior and exterior so defined is equivalent to Connolly's definition of the molecular surface.[25] No counterions were included, which assumed that the ionic strength is 0. The resulting Poisson equation was solved by using an overrelaxation algorithm[23] on successively finer grids of size 61^3, 61^3, and 81^3 with linear spacings of 1.0, 0.25, and 0.15 Å, respectively. Subtracting the potential calculated in this way from the vacuum potential, which was calculated with $\epsilon_i = \epsilon_o = 1$, yielded the net solvent reaction field potential that was added to the molecular Hamiltonian in the self-consistent density functional calculation. The cycle of ESP fitting, reaction field calculation and density functional calculation was repeated until full convergence of the molecular energy was achieved. The solvation energy was determined from the difference between the molecular energies in the solvent and in gas-phase states. A more detailed description of the methodology can be found elsewhere.[6a,b]

4. Cluster Models. Within the solute region where a discrete cluster model was needed, we adopted a cluster $[M(H_2O)_6]^{m+}$ ($m = 2, 3$; M = Mn, Fe) as the first hydration shell model (Figure 1a). The structure of the cluster was determined through gas-phase geometry optimization by the density functional method. In order to examine the effects of the second hydration shell, 12 water molecules were added to the $[M(H_2O)_6]^{m+}$ cluster forming hydrogen bonds to the waters in the first shell. The distances and angles between the first and second shell waters in the large cluster $[M(H_2O)_{18}]^{m+}$ were optimized using the Discover module in Insight II (Biosym Technologies, Inc.). The configuration of the large cluster is shown in Figure 1b. Similar techniques were applied to build the structures of the clusters $[M(OH)(H_2O)_5]^{(m-1)+}$ and $[M(OH)(H_2O)_{17}]^{(m-1)+}$, in which one water molecule in the first shell is deprotonated (Figure 1c,d).

Table 1. M−O distances (in Å) in $[M(H_2O)_6]^{m+}$

	expt[a]	DFT-(NL)[b]	DFT-(LDA)[c]	ab initio[d]
$[Mn(H_2O)_6]^{2+}$	2.175[e] (2.17−2.20)	2.197 (6)	2.121 (6)	2.233 (6)
$[Mn(H_2O)_6]^{3+}$	1.991[f]	1.952 (4)		1.99 (4)
		2.114 (2)		2.15 (2)
$[Fe(H_2O)_6]^{2+}$	2.126[e] (2.10−2.28)	2.127 (4)	2.070 (4)	2.185 (6)
		2.132 (2)	2.075 (2)	
$[Fe(H_2O)_6]^{3+}$	1.995[f] (1.99−2.06)	2.067 (6)		2.062 (6)

[a] Data in parentheses represent the M−O distance ranges observed by other experiments.[26a] [b] This work. The number of equivalent distances is indicated in parentheses. [c] Using the DGauss program with (12s9p5d)/[5s3p2d] GTO basis sets for transition metals, (9s5p1d)/[3s2p1d] basis set for oxygen, and (5s)/[2s] for hydrogen.[28] [d] Geometry optimized at HF-SCF level. Relativistic ECP and [5s4p3d] basis sets for transition metals and [9s5p] and [4s] basis sets for oxygen and hydrogen, respectively.[27d] [e] Tutton salt, mean M−O value.[29a] [f] Alum salt, mean M−O value.[29b]

Results and Discussion

1. Gas-Phase Geometry Optimization. Scattering and spectroscopic methods, such as X-ray or neutron diffraction, EXAFS, XANES, and NMR, have been extensively applied to probe the structure of the first hydration shells of metal cations.[26] The determination of hydration numbers shows that there are six water molecules in the first hydration shell of most di- or trivalent transition metal cations. The $[M(H_2O)_6]^{m+}$ cluster is thus a reasonable static model for the first solvent coordination shell. Åkesson *et al.* carried out a series of ab initio calculations on $[M(H_2O)_6]^{m+}$ for first- and second-row transition metals at the HF-SCF level with medium-sized basis sets and effective core potentials (ECP).[27] Waizumi *et al.* also reported a local spin density functional calculation on these same clusters.[28] Following this work, the starting conformation for geometry optimization was one with T_h symmetry. During the course of optimization, Jahn−Teller effects decreased the symmetry to D_{2h} in Mn^{3+} and Fe^{2+} cases. As a constraint, the orientations of the water molecules were retained. The internal water geometry was kept rigid at gas phase values (O−H bond distance 0.958 Å and H−O−H angle 104.5°), as optimized by the current density functional method. The optimized M−O distances, together with available experimental values[29] and other calculated data, are summarized in Table 1.

As demonstrated in Table 1, the density functional optimized M−O distances in $[M(H_2O)_6]^{m+}$ are in good agreement with experiment, lying within the range of experimental values. (The experimental values vary to some extent depending on counterions and measurement methods.[26]) Compared to other theoretical values, density functional calculations using DGauss at the LDA level gave consistently shorter M−O distances for

(25) Connolly, M. L. *Science* **1983**, *221*, 709.

(26) (a) Ohtaki, H.; Radnai, T. *Chem. Rev.* **1993**, *93*, 1157. (b) Magini, M.; Licheri, G.; Paschina, G.; Piccaluga, G.; Pinna, G. *X-ray Diffraction of Ions in Aqueous Solutions: Hydration and Complex Formation*; CRC Press: Boca Raton, FL, 1988.

(27) (a) Åkesson, R.; Pettersson, L. G. M.; Sandström, M.; Wahlgren, U. *J. Phys. Chem.* **1992**, *96*, 150. (b) Åkesson, R.; Pettersson, L. G. M.; Sandström, M.; Siegbahn, P. E. M.; Wahlgren, U. *J. Phys. Chem.* **1992**, *96*, 10773. (c) Åkesson, R.; Pettersson, L. G. M.; Sandström, M.; Siegbahn, P. E. M.; Wahlgren, U. *J. Phys. Chem.* **1993**, *97*, 3765. (d) Åkesson, R.; Pettersson, L. G. M.; Sandström, M.; Wahlgren, U. *J. Am. Chem. Soc.* **1994,** *116*, 8691. (e) Åkesson, R.; Pettersson, L. G. M.; Sandström, M.; Wahlgren, U. *J. Am. Chem. Soc.* **1994**, *116*, 8705.

(28) Waizumi, K.; Ohtaki, H.; Masuda, H.; Fukushima, N.; Watanabe, Y. *Chem. Lett.* **1992,** 1489.

(29) (a) Cotton, F. A.; Daniels, L. M.; Murillo, C. A.; Quesada, J. F. *Inorg. Chem.* **1993**, *32*, 4861. (b) Best, S. P.; Forsyth, J. B. *J. Chem. Soc., Dalton Trans.* **1991**, 1721.

Table 2. Bond Lengths[a] (in Å) in $[M(H_2O)_{18}]^{m+}$

		calc	expt[b]
$[Mn(H_2O)_{18}]^{2+}$	Mn−O(1)	2.204	2.17−2.20
	Mn−O(2)	4.433	4.17−4.43
	O(1)−O(2)	2.693	2.71−2.78
	H(1)···O(2)	1.735	
$[Mn(H_2O)_{18}]^{3+}$	Mn−O(1)	1.992, 2.154	
	Mn−O(2)	4.194, 4.327	
	O(1)−O(2)	2.613	
	H(1)···O(2)	1.666	
$[Fe(H_2O)_{18}]^{2+}$	Fe−O(1)	2.162, 2.170	2.095−2.28
	Fe−O(2)	4.374, 4.379	4.30−4.51
	O(1)−O(2)	2.694	2.84−2.87
	H(1)···O(2)	1.736	
$[Fe(H_2O)_{18}]^{3+}$	Fe−O(1)	2.069	1.99−2.05
	Fe−O(2)	4.273	4.09−4.80
	O(1)−O(2)	2.627	2.621−2.77
	H(1)···O(2)	1.670	

[a] M−O(1) distance readjusted by DFT point calculations. Mean M−O(2), O(1)−O(2), and H(1)−O(2) distances determined by molecular mechanics method. [b] Reference 26a.

the two divalent complexes. This is not surprising, since LDA methods generally tend to underestimate bond lengths.[8] The ab initio results agree with the NL density functional ones reasonably well. Jahn−Teller distortions are found for d^4 $[Mn(H_2O)_6]^{3+}$ and d^6 $[Fe(H_2O)_6]^{2+}$ in both the DFT and ab initio calculations. We observe an axial elongation in $[Mn(H_2O)_6]^{3+}$ and $[Fe(H_2O)_6]^{2+}$, with energy gains of 2.2 and 1.6 kcal/mol, respectively. Such shallow wells and axial elongations were reported in other calculations as well. Ab initio calculations showed a gain in energy of 2.8 kcal/mol for $[Mn(H_2O)_6]^{3+}$.[27b]

Experimental information on the structural details of the second hydration shell is scarce and uncertain compared with that for the first shell. X-ray diffraction measurements of some di- and trivalent manganese and iron salts suggest that the hydration number is about 12.[26] This has been supported by several molecular simulation analyses.[30a−c] The arrangement of these 12 water molecules is not clear, however, and a full geometry optimization of the whole cluster $[M(H_2O)_{18}]^{m+}$ by the density functional method is currently not feasible. Since direct bonding between the metal center and the second-shell water molecules is relatively weak, the location is determined mainly by hydrogen-bonding and steric interactions. Starting from the optimized $[M(H_2O)_6]^{m+}$ structure, we positioned the 12 second-shell water molecules in such a way that each binds to only one hydrogen atom from a water molecule in the first shell with the second shell oxygen atoms oriented toward the corresponding hydrogen atom. The larger cluster preserved the symmetry of the smaller one, and the H(1)···O(2) distances were optimized using Discover. After the outer shell was constructed, the inner shell was allowed to breathe over a small range and the M−O(1) distances were then readjusted by a quadratic fitting based on several single-point density functional energy calculations. The structural relaxation of the first hydration shell in response to the second hydration shell was thus included in the $[M(H_2O)_{18}]^{m+}$ cluster model. The readjusted M−O(1) distances and other geometry parameters of $[M(H_2O)_{18}]^{m+}$ are shown in Table 2.

The most pertinent parameters in Table 2 are M−O(2) and O(1)−O(2) distances. Again, the calculated values compare fairly well with experimental ones. Due to the flexibility of the water molecules in the second shell, the experimental M−O(2) distances span a wide range.[26] All of the calculated M−O(2) lengths lie within this range. The calculated data show that O(1)−O(2) distances in the trivalent complexes are shorter than those in the divalent complexes. This observation is confirmed by experiment. The average H(1)···O(2) distances are in the typical hydrogen-bond range. Comparing the M−O(1) lengths in Table 2 with Table 1 reveals that, in the presence of the second hydration shell, the first shell expands slightly. The inner shells with d^5 metal cations are more rigid than the others, with a M−O(1) bond lengthening of less than 0.01 Å, while for d^4 and d^6 cations the average lengthening is about 0.04 Å. Furthermore, the energy gain from the structural expansion is very marginal, only 0.4−0.8 kcal/mol. Thus, the discrete cluster models optimized in gas phase should not deviate much from those in solution phase. Marcos *et al*., who studied the effects of the solvent reaction field on the geometry of several hexahydrated metallic cations by means of a gradient analytical method,[5d] observed that the solvent reaction field lengthens the M−O distance by only 0.02−0.05 Å.

Table 3. Calculated Geometry Parameters[a] in $M(OH)(H_2O)_{17}^{(m-1)+}$

	$Mn(OH)(H_2O)_{17}^{+}$	$Mn(OH)(H_2O)_{17}^{2+}$	$Fe(OH)(H_2O)_{17}^{+}$	$Fe(OH)(H_2O)_{17}^{2+}$
M−O*[b]	1.870	1.729	1.799	1.787
M−O*−H[b]	128	123	128	132
O*−H[b]	0.978	0.993	0.978	0.995
O*···H[b]	1.851	2.151	1.796	2.143
M−O(1)[c]	2.240	2.105	2.242	2.131
	2.352	2.185	2.310	2.183
M−O(2)	4.545	4.358	4.536	4.365
O(1)···O(2)	2.694	2.641	2.693	2.627
H···O(2)	1.737	1.684	1.733	1.671

[a] Distances in Å and angles in deg. [b] O* represents the oxygen in the hydroxo group. [c] The first number corresponds to distance of the M−O(1) trans to M−O*H. The second number is the mean distance value of the other M−O(1) cis to M−O*H.

The deprotonated clusters possess only C_s symmetry. In addition to the M−O distances, the O−H lengths and M−O−H angles of the hydroxide groups are listed in Table 3. No direct comparison to the experimental structure can be made due to the lack of experimental data. Since the hydroxide group is in the inner shell, one of the second-shell water molecules flips over to form a strong hydrogen bond to the O−H group and the second shell structure in $[M(OH)(H_2O)_{17}]^{(m-1)+}$ changes accordingly (see Figure 1d). Some of optimized geometrical parameters for the large clusters are shown in Table 3 as well. We did not repeat the readjustment of the M−O(1) distances in the inner shell to obtain the marginal energy gain from the structural breathing mode.

Due to the flexibility of the water molecules in the second hydration shell, the highly symmetrical model we have chosen for large clusters represents only one of many possible configurations for the second-shell structure. It may not correspond to the global minimum in potential energy surface. This could introduce an error to the internal energy of the cluster. However, since a consistent symmetry constraint was imposed on the clusters with different charges and the water−water repulsion in the second shell was minimized by force field methods, we expect that such a single configuration model can reasonably account for the effects of the second hydration shell in reduction and deprotonation procedures. Further, our main focus is on the energy differences needed to calculate redox potentials and pK_a's. To sample more configurations, a molecular dynamics (MD) scheme has to be employed. For instance, King and Warshel used a three-region model to represent an ion surrounded by a sphere of polar solvent molecules and implemented proper surface or polarization

(30) (a) Zeng, J.; Crow, J. S.; Hush, N. S.; Reimers, J. R. *J. Phys. Chem*. **1994,** *98*, 11075. (b) Clementi, E.; Barsotti, R. *Chem. Phys. Lett.* **1978**, *59*, 21. (c) Radnai, T.; Palinkas, G.; Szasz, G. I.; Heinzinger, K. *Z. Naturforsch*. **1987**, *A36*, 1076. (d) King, G.; Warshel, A. *J. Chem. Phys*. **1989,** *91*, 3647.

Table 4. Energetics of $[M(H_2O)_6]^{m+}$ and $[M(H_2O)_{18}]^{m+}$ in Gas Phase and Solution[a]

	$\Delta E_b^{(1)}(M-H_2O)$[b]		$\Delta E_b^{(2)}(M-H_2O)$[c]	ΔE_{sol}		$\Delta H_{hyd}°$		
	DFT	ab initio[d]	DFT	$[M(H_2O)_6]^{m+}$	$[M(H_2O)_{18}]^{m+}$	$[M(H_2O)_6]^{m+}$	$[M(H_2O)_{18}]^{m+}$	expt[e]
Mn^{2+}	47.4	47.0	12.1	−197.9	−158.1	424	409	440
Mn^{3+}	111.8	102.5	22.7	−449.9	−308.2	1062	1073	1087
Fe^{2+}	50.9	49.6	12.2	−198.6	−158.5	445	431	465
Fe^{3+}	108.7	99.6	22.2	−443.9	−306.7	1037	1046	1060

[a] Energy in kcal/mol. [b] Calculated according to eq 1. [c] Calculated according to eq 2. [d] See footnote *d* in Table 1.[27d] [e] Reference 33.

constraints.[30d] In this way, the effects of a second or third hydration shell and the solvent reaction field, which have been found significant both for geometry and energetics, can be included in the MD simulations. However, implementation of this in conjunction with a good SCF field and geometry optimization of the first- and second-shell waters is a difficult computational task, and has not been attempted in our work.

2. Gas-Phase and Solvation Energetics. For hydrated metal cations, the water molecules play a role not only as solvent but also as the ligands in the inner shell, binding tightly to the metal center.[31] In the combined discrete−continuum model, the total solvation or hydration energy is made up of both the discrete and the continuum contributions. In order to calculate the properties of metal cations, both components must be computed accurately, and calibrations are necessary.

The binding strength of the first-shell water molecules to a metal center can be related to the gas-phase average binding energy $\Delta E_b^{(1)}(M-H_2O)$ in the cluster $[M(H_2O)_6]^{2+/3+}$ by

$$\Delta E_b^{(1)}(M-H_2O) = {}^1/_6\{E[M^{m+}(g)] + 6E[H_2O(g)] - E[M(H_2O)_6{}^{m+}(g)]\} \quad (1)$$

The density functional calculated values of $\Delta E_b^{(1)}(M-H_2O)$ are listed in Table 4, together with the ab initio results[27d] for comparison. For divalent complexes, the DFT and ab initio results compare very well. For trivalent complexes, the DFT values are about 9 kcal/mol larger. The lack of correlation and the modest size of the HF basis set of the ab initio calculations, which were carried out at the HF-SCF level, might be the reason for the discrepancy, especially because there are highly charged complexes where more flexible basis sets are needed.

The binding energy contribution from each water molecule in the second shell is calculated according to

$$\Delta E_b^{(2)}(M-H_2O) = {}^1/_{12}\{12E[H_2O(g)] + E[M(H_2O)_6{}^{m+}(g)] - E[M(H_2O)_{18}{}^{m+}(g)]\} \quad (2)$$

These calculated values are included in Table 4 as well. $\Delta E_b^{(2)}(M-H_2O)$ is the result of the bonding interaction between the metal cations and water molecules in the second shell and hydrogen bonding between the first and second shells. The calculated $\Delta E_b^{(2)}(M-H_2O)$ values show that the bonding interaction between the second-shell water molecules and the metal center is rather weak for the divalent cations, with only a few kcal/mol change after subtracting $\Delta E_b^{(2)}(M-H_2O)$ from the normal hydrogen bond strength (5−7 kcal/mol per H-bond) in water clusters.[32] For the trivalent cations, the $\Delta E_b^{(2)}(M-H_2O)$ values suggest either a nonnegligible bonding between the metal center and the second-shell water molecules or strong hydrogen bonds between the first and second shells.

The hydration enthalpy of metal cations can be determined by thermochemical methods.[33] In order to relate the calculated quantities to the experimental hydration enthalpy ($\Delta H°_{hyd}$) at 298 K, correction terms have to be considered as follows:

$$-\Delta H°_{hyd} = -\Delta E_b + \Delta E_{sol} + n\Delta H_{vap} + \Delta nRT - \Delta E(Cp) - \Delta E_{zp} + \Delta E_{rel} + \Delta E_{geom} \quad (3)$$

ΔE_b is the total binding energy of the gas phase cluster $[M(H_2O)_6]$ or $[M(H_2O)_{18}]$, which is $6\Delta E_b^{(1)}$ and $[12\Delta E_b^{(2)} + 6\Delta E_b^{(1)}]$, respectively. ΔE_{sol} represents the calculated solvation free energy of the cluster corresponding to the procedure $[M(H_2O)_n{}^{m+}(g)] \rightarrow [M(H_2O)_n{}^{m+}(aq)]$, listed in Table 4. This term contains the entropic contribution to the solvation free energy for the continuum dielectric part. We neglect this contribution in eq 3 and Table 4. ΔH_{vap} is the heat of vaporization of water. Density functional calculations on the clusters $(H_2O)_6$ and $(H_2O)_{18}$ give average vaporization energies of 8.61 and 11.05 kcal/mol,[32b] respectively. Here the experimental ΔH_{vap} value[34] of 10.67 kcal/mol is used in eq 3. The $\Delta E(Cp)$ term arises from the difference in heat capacity of the components of the system, which is a small correction of about 1 kcal/mol at 298 K. An estimate of ΔE_{zp}, the difference in vibrational zero-point energy in forming the clusters, requires calculation of the vibrational frequencies of the clusters, which is too expensive for systems like $[M(H_2O)_{18}]$. ΔE_{rel} and ΔE_{geom} are corrections due to relativistic effects for metal centers and geometry relaxation for H_2O during the formation of the clusters. ΔE_{zp} usually reduces the total binding energy by a few kcal/mol, while ΔE_{rel} and ΔE_{geom} increase ΔE_b comparably. On the whole, these three terms tend to cancel to some extent and they are not included in the calculated $\Delta H°_{hyd}$ values in Table 4.

The agreement between the calculated and experimental $\Delta H°_{hyd}$ values is very impressive. For divalent cations, even the small cluster model reproduces the experimental measurements very well. For trivalent cations, the larger clusters including the second shells bring the calculated data closer to the experimental results. These results indicate that the methods and cluster models outlined here provide a reasonable approach to studying cations both in gas phase and in solution. However, the current method and model cannot account for the fluctuations in solvation energy, ΔE_{sol}, and internal energy, arising from configurational variations, especially for larger clusters. Such effects might be evaluated by quantum molecular dynamics or Monte Carlo simulation, which is too expensive to be coupled into the conventional density functional calculations. Recently, Wesolowski and Warshel developed a free energy perturbation scheme using the frozen density functional approach. This method seems feasible to treat large clusters with many explicit solvent water molecules in hydration shells, although charge

(31) (a) Marcus, Y. *Chem. Rev.* **1988**, *88*, 1475. (b) Marcus, Y. *Ion Solvation*; Wiley: Chichester, U.K., 1986. (c) Richens, D. T. *Perspect. Bioinorg. Chem.* **1993**, *2*, 245.

(32) (a) Suhai, S. *J. Phys. Chem.* **1995**, *99*, 1173. (b) Lee, C.; Chen, H.; Fitzgerald, G. *J. Chem. Phys.* **1994**, *101*, 4472.

(33) (a) Rosseinsky, D. R. *Chem. Rev.* **1965**, *65*, 467. (b) Smith, D. W. *J. Chem. Educ.* **1977**, *54*, 540.

(34) Lide, D. R. *Handbook of Chemistry and Physics*, 73rd ed.; CRC Press: Boca Raton, FL, 1972.

Scheme 1

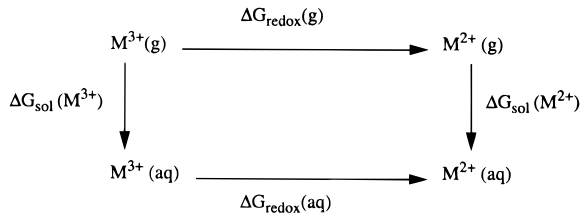

transfer to the frozen density water molecules is not allowed.[35] In the next sections, we only use the solvation energy difference $\Delta\Delta E_{sol}$ to calculate redox potentials and pK_a values. The effect of structural fluctuations is expected to be cancel to some extent.

Rough estimates of the solvation energy of ions or spherical clusters can be made by the Born equation.[30d,36] Åkesson *et al.*[27d] used this approximation to calculate the solvation energy corresponding to $[M(H_2O)_6^{m+}(g)] \rightarrow [M(H_2O)_6^{m+}(aq)]$. By choosing certain cavity radii, they obtained values of −222 kcal/mol for $[Mn(H_2O)_6]^{2+}$ and −540 kcal/mol for $[Mn(H_2O)_6]^{3+}$. Compared to our calculated ΔE_{sol} values in Table 4, the Born equation results are too negative. The deviations for $[Mn(H_2O)_6]^{2+}$ and $[Mn(H_2O)_6]^{3+}$ are −24 and −90 kcal/mol, respectively.

3. Redox Potentials. The gas phase and solution energetic data in Table 4 enable us to compute the redox potentials for Mn^{2+}/Mn^{3+} and Fe^{2+}/Fe^{3+} in aqueous solution. The calculation is based on the thermodynamic cycle shown in Scheme 1. The overall reaction in aqueous solution is characterized by the standard Gibbs free energy

$$\Delta G_{redox}(aq) = \Delta G_{redox}(g) + \Delta G_{sol}(M^{3+}) - \Delta G_{sol}(M^{2+}) \quad (4)$$

and the redox potential is thus related to $\Delta G_{redox}(aq)$ as

$$\Delta G_{redox}(aq) = -FE_{redox}^{\circ} \quad (5)$$

where F is the Faraday constant, 23.06 kcal mol^{-1} V^{-1}. By using calculated gas phase ionization potentials IP(g) and differences in solvation energy $\Delta\Delta E_{sol}$ (reduced − oxidized species), the redox potential E_{redox}° can be calculated according to

$$E_{redox}^{\circ} = IP(g) - \Delta\Delta E_{sol} + T\Delta S(aq) + \Delta SHE + \Delta E_{rel} + \Delta E_{geom} \quad (6)$$

with all terms in units of eV. ΔSHE represents the standard hydrogen electrode potential of −4.43 eV.[37] ΔE_{rel} and ΔE_{geom} are the relativistic and geometry relaxation corrections to the IP(g)s. ΔE_{geom} is estimated from another density functional calculation for a $[M(H_2O)]_6^{m+}$ cluster in which the O−H distance and H−O−H angle for the ligated H_2O molecules are optimized. In general, the O−H distance is observed to be lengthened and H−O−H angle to be opened slightly. In $Mn(H_2O)_6^{2+}$ and $Fe(H_2O)_6^{3+}$, in which the six water molecules are geometrically equivalent, the O−H bond lengths increase by 0.023 and 0.032 Å and H−O−H angles increase by 1.5 and 2.0°, respectively, compared with the optimized gas-phase values. In $Mn(H_2O)_6^{3+}$, the O−H bonds lengthen by 0.033 and 0.030 Å, the H−O−H angles open by 3.5 and 0.5°, respectively, for the four equatorial water ligands and two axial water ligands. Similarly, the changes in $Fe(H_2O)_6^{2+}$ are 0.019 and 0.017 Å for O−H distances and 1.0 and 0.6° for H−O−H angles. We assume that the energy gained from such a relaxation is the same for the $[M(H_2O)]_{18}^{m+}$ cluster. The calculated E_{redox}° and other terms in (6) are tabulated in Table 5.

The experimental third ionization potentials for Mn and Fe atoms are 33.7 and 30.7 eV, respectively.[38] Our calculated values correspond to the energy differences between the states Mn^{2+}-(^{6}S) and Mn^{3+}(^{5}D), Fe^{2+}(^{5}D) and Fe^{3+}(^{6}S). Taking into account the relativistic corrections, the calculated values are 34.3 and 31.6 eV for Mn and Fe, respectively, giving an absolute error of 0.6−1.1 eV and a relative error of 2−4%.[39] The experimental entropies of Fe^{2+}(aq) and Fe^{3+}(aq) are estimated to be −108 and −286 J K^{-1} mol^{-1}, and thus the $T\Delta S$ for $Fe^{3+}(aq) \rightarrow Fe^{2+}$-(aq) at 298 K is 0.55 eV.[40] We use this value for $Mn^{3+}(aq) \rightarrow Mn^{2+}(aq)$ as well as for all other cluster cases.

The experimental redox potentials for Mn^{2+}/Mn^{3+} and Fe^{2+}/Fe^{3+} pairs are 1.56 and 0.77 V, respectively.[35] When the DFT calculations are carried out on naked metal cations in a continuum solvent, the E_{redox}° obtained deviate from the experimental data by 2−4 eV. Since the continuum solvation energy is a free energy and therefore includes entropy, no empirical entropy correction is made for naked metal ions in the continuum solvent. The small cluster model including the first hydration shell brings the calculated values closer to the experimental ones with a deviation about 1 V. Inclusion of the second hydration shell greatly improves the calculation, resulting in deviations of less than 0.3 eV. Figure 2 depicts the convergence toward experimental values. The similarity between the final computed value and the experimental one for Mn^{2+}/Mn^{3+} may be somewhat fortuitous, as the experimental value was measured at high salt concentration[41] while our calculations assumed a solution with zero ionic strength.[40c] Nevertheless, with a proper cluster model, the current method yields redox potentials that are accurate to about 200−400 mV.[9] Recent calculations of E_{redox}° by this method for a model of the active site in human mitochondrial superoxide dismutase (MnSOD) obtained a value of +0.17 V, compared with experimental values of +0.26 V for MnSOD from *Bacillus stearothermophilus* and +0.31 V from *Escherichia coli* Mn-SOD,[10] although the possibility of coupled protonation on reduction complicated the analysis of this result. Wheeler has reported that in calculations on *p*-benzoquinone by a hybrid Hartree−Fock/density functional and thermodynamic perturbation/molecular dynamics method, the calculated one-electron redox potential was accurate to 100 mV.[42]

4. Absolute pK_a Values. The solvated metal cations, especially the highly charged ones, can deprotonate a coordinated water molecule to form a hydroxo ligand. Such deprotonations have often been postulated to explain the hydrolytic

(35) (a) Wesolowski, T. A.; Warshel, A. *J. Phys. Chem.* **1993**, *97*, 8050. (b) Wesolowski, T. A.; Warshel, A. *J. Phys. Chem.* **1994**, *98*, 5183.
(36) (a) Krauss, M.; Stevens, W. J. *J. Am. Chem. Soc.* **1990**, *112*, 1460. (b) Garmer, D. R.; Krauss, M. *J. Am. Chem. Soc.* **1992**, *114*, 6487.
(37) Reiss, H.; Heller, A. *J. Phys. Chem.* **1985**, *89*, 4207.
(38) Moore, C. E. *Atomic Energy Level*; Natl. Bur. Stand.: Washington, DC, 1958.
(39) (a) Becke, A. D. *J. Chem. Phys.* **1993**, *98*, 5648. (b) Russo, T. V.; Martin, R. L.; Hay, P. J. *J. Chem. Phys.* **1994**, *101*, 7729. (c) Eriksson, L. A.; Pettersson, L. G.; Siegbahn, P. E. M.; Wahlgren, U. *J. Chem. Phys.* **1995,** *102,* 872.
(40) (a) Johnson, D. A. *Some Thermodynamic Aspects of Inorganic Chemistry*, 2nd ed.; Cambridge University Press: Cambridge, U.K., 1982. (b) Atkins, P. W. *Physical Chemistry*, 2nd ed.; Freeman: San Francisco, CA, 1982. (c) Most redox potential calculations include an empirical correction for the salt concentration extrapolating to zero concentration based on Debye-Hückel theory. [40b] This should remove some of the inconsistency between our calculations and experiment. (d) Again, corrections based on extended Debye−Huckel theory will decrease but not eliminate this discrepancy for acidities at high ionic strength.
(41) Cotton, F. A.; Wilkinson, G. *Advanced Inorganic Chemistry*, 5th ed.; Wiley: New York, 1988.
(42) Wheeler, R. A. *J. Am. Chem. Soc.* **1994**, *116*, 11048.

Table 5. Calculated and Experimental Redox Potentials[a]

	IP_{red}(g)	$\Delta\Delta E_{sol}$	$T\Delta S$	ΔE_{rel}	ΔE_{geom}	$E_{redox}°$(calc)	$E_{redox}°$(exp)
$Mn^{3+} + e \rightarrow Mn^{2+}$	34.52	24.58		−0.21		5.30	
$Mn(H_2O)_6^{3+} + e \rightarrow Mn(H_2O)_6^{2+}$	17.76	10.93	0.55	−0.11	−0.18	2.66	
$Mn(H_2O)_{18}^{3+} + e \rightarrow Mn(H_2O)_{18}^{2+}$	12.27	6.51	0.55	−0.11	−0.18	1.59	1.56[b]
$Fe^{3+} + e \rightarrow Fe^{2+}$	31.81	24.56		−0.21		2.61	
$Fe(H_2O)_6^{3+} + e \rightarrow Fe(H_2O)_6^{2+}$	16.78	10.64	0.55	−0.09	−0.17	2.00	
$Fe(H_2O)_{18}^{3+} + e \rightarrow Fe(H_2O)_{18}^{2+}$	11.63	6.43	0.55	−0.09	−0.17	1.06	0.77[c]

[a] $E_{redox}°$ in V and other terms in eV. [b] References 35 and 41. Measured in 3 M $LiClO_4$. [c] Reference 35.

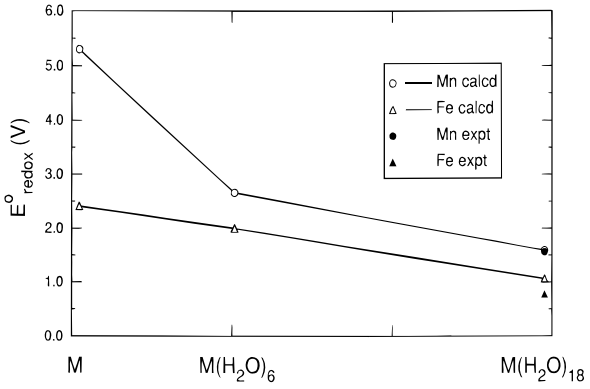

Figure 2. Convergence of calculated one-electron redox potentials with increasing size of cluster models.

Scheme 2

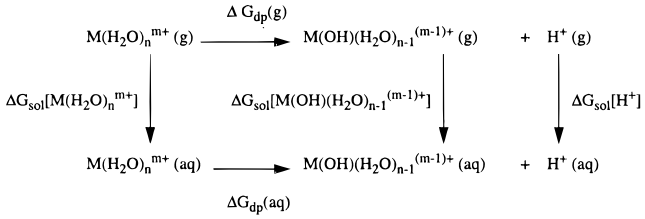

mechanisms of metalloenzyme catalysis,[43a] and some quantum chemical calculations on this deprotonation process in enzymes like carbonic anhydase have been reported.[43b] If only one of the first-shell water molecules is deprotonated, the absolute pK_a value, or the measurement of the capacity of deprotonation or the acidity of the metal cations, can be calculated on the basis of the thermodynamic cycle shown in Scheme 2 from the equation

$$1.37\mathrm{p}K_a = \Delta G_{dp}(aq) = -\Delta G_{sol}[M(H_2O)_n^{m+}] + \Delta G_{dp}(g) + \Delta G_{sol}[M(OH)(H_2O)_{n-1}^{(m-1)+}] + \Delta G_{sol}[H^+] \quad (7)$$

By using the calculated proton affinity, PA(g), of $[M(OH)(H_2O)_{n-1}]^{(m-1)+}$ and the solvation energy, ΔE_{sol}, of clusters $[M(H_2O)_n]^{m+}$ and $[M(OH)(H_2O)_{n-1}]^{(m-1)+}$, eq 7 becomes

$$1.37\mathrm{p}K_a = \mathrm{PA(g)} - \Delta E_{sol}[M(H_2O)_n^{m+}] + \Delta E_{sol}[M(OH)(H_2O)_{n-1}^{(m-1)+}] - 267.7 \text{ kcal/mol} \quad (8)$$

where −267.7 kcal/mol corresponds to the sum of the solvation free energy of the proton (−260.5 kcal/mol), which is estimated from the absolute potential correction for the standard hydrogen electrode, ΔSHE = −4.43 eV,[37] plus the translational entropy contribution to the free energy of a proton, −7.2 kcal/mol at 300 K. One approximation introduced here is the assumption that the internal entropies of the clusters $[M(H_2O)_n]^{m+}$ and $[M(OH)(H_2O)_{n-1}]^{(m-1)+}$ are similar and approximately cancel out. The internal vibrational/configurational entropy should increase as the net cluster charge decreases. However, the shorter metal−hydroxyl oxygen bond length (see Tables 2 and 3) in the deprotonated form should lead to significantly lower entropy for this bond. Which of these two compensating effects is larger is not clear.

Table 6. Calculated Vibrational Frequencies and Vibrational Zero-Point Energies of $M(H_2O)^{m+}$ and $M(OH)^{(m-1)+}$ [a]

	frequency	E_{zp}
$Mn(H_2O)^{2+}$	460 (a_1), 1616 (a_1), 3551 (a_1), 636 (b_1), 3381 (b_1), 504 (b_2)	14.5
$Mn(OH)^+$	408, 761, 3586	6.8
$Mn(H_2O)^+$	420 (a_1), 1572 (a_1), 3580 (a_1), 452 (b_1), 3646 (b_1), 203 (b_2)	14.1
Mn(OH)	622, 681, 3580	7.0

[a] Frequencies in cm^{-1} and E_{zp} in kcal/mol.

The proton affinity is calculated from the total binding energy difference, $\Delta\Delta E_b$, of the species $[M(H_2O)_n]^{m+}$, $[M(OH)(H_2O)_{n-1}]^{(m-1)+}$, and a proton with several correction terms

$$\mathrm{PA(g)} = \Delta\Delta E_b + \Delta E_{zp} + {}^5/_2RT + \Delta E_{rel} + \Delta E_{geom} + \Delta E_{BSSE} \quad (9)$$

The relativistic effects only equate to about −0.1 kcal/mol, as the bond broken is not directly bonded to the metal center. The energy ΔE_{BSSE} from the basis set superposition error (BSSE) is expected to be insignificant, although it can be estimated by a counterpoise correction.[6a] The size of the clusters prevent an accurate estimate of vibrational zero point energy difference based on frequency calculations. Given that the lost vibrational freedom in the deprotonated cluster is pertinent mainly to the O−H bond in the ligated water molecule, the zero point energy difference between monoaquo and monohydroxo complexes gives a good approximation for ΔE_{zp}. In view that there are fewer ligated waters in the monoaquo and monohydroxo models, and in order to correctly account for the effective net charge in the metal centers, we assign a lower net charge to the clusters. That is, $M(H_2O)^+$ simulates $[M(H_2O)_6]^{2+}$, while $M(H_2O)^{2+}$ simulates $[M(H_2O)_6]^{3+}$. A similar strategy applies to M(OH) and $M(OH)^+$. The final calculated harmonic frequencies of $M(H_2O)^{n+}$ and $M(OH)^{(n-1)+}$ are listed in Table 6. The calculated pK_a values derived with these frequencies and relevant terms in eqs 8 and 9 are summarized in Table 7.

The experimental pK_a values determined by potentiometric titrations[44] are available for Mn^{2+}, Mn^{3+}, Fe^{2+}, and Fe^{3+}. All of these values were determined at different ionic strengths.

(43) (a) Lippard, S. J.; Berg, J. M. *Principles of Bioinorganic Chemistry;* University Science Books: Mill Valley, CA, 1994. (b) Åqvist, J.; Warshel, A. *Chem. Rev.* **1993**, *93*, 2523.

(44) (a) Yatsimirksii, K. B.; Vasil'ev, V. P. *Instability Constants of Complex Compounds*; Pergamon: New York, 1960. (b) Baes, C. J.; Mesmer, R. E. *The Hydrolysis of Cations*; Krieger: Malabar, India, 1986. (c) Fontano, S.; Brito, F. *Inorg. Chim. Acta* **1968**, *2*, 179. (d) Macartney, D. H.; Sutin, N. *Inorg. Chem.* **1985,** *24*, 3403. (e) Flynn, C. M., Jr. *Chem. Rev.* **1984**, *84*, 31.

Table 7. Absolute pK_a Values of Hydrated Metal Cations[a]

	$\Delta\Delta E_b$	ΔE_{zp}	ΔE_{geom}	$\Delta E_{sol}[M(OH)(H_2O)_{n-1}]$[b]	pK_a(calc)	pK_a(exp)
$Mn(H_2O)_6^{2+} \rightarrow Mn(OH)(H_2O)_5^{+} + H^+$	154.6	−7.1	+1.2	−78.4	1.4	
$Mn(H_2O)_{18}^{2+} \rightarrow Mn(OH)(H_2O)_{17}^{+} + H^+$	234.5	−7.1	+1.2	−101.2	14.0	10.6[c]
$Mn(H_2O)_6^{3+} \rightarrow Mn(OH)(H_2O)_5^{2+} + H^+$	11.6	−7.7	+4.4	−206.7	−10.8	
$Mn(H_2O)_{18}^{3+} \rightarrow Mn(OH)(H_2O)_{17}^{2+} + H^+$	124.8	−7.7	+4.4	−172.4	−6.5	0.1[d]
$Fe(H_2O)_6^{2+} \rightarrow Fe(OH)(H_2O)_5^{+} + H^+$	152.6	−7.1	+0.6	−74.3	3.1	
$Fe(H_2O)_{18}^{2+} \rightarrow Fe(OH)(H_2O)_{17}^{+} + H^+$	228.2	−7.1	+0.6	−101.7	9.0	9.5[e]
$Fe(H_2O)_6^{3+} \rightarrow Fe(OH)(H_2O)_5^{2+} + H^+$	18.7	−7.7	+3.9	−206.7	−10.5	
$Fe(H_2O)_{18}^{3+} \rightarrow Fe(OH)(H_2O)_{17}^{2+} + H^+$	132.5	−7.7	+3.9	−174.7	−4.0	2.2[f]

[a] Energy terms in kcal/mol and pK_a's in pH units. [b] $\Delta E_{sol}[M(H_2O)_n]$ can be found in Table 4. [c] In 1 M Na_2SO_4.[44c] [d] In 2 M $LiClO_4$.[44d] [e] In alkaline solution.[44b] [f] Ionic strength $\mu = 0$.[44e]

From the cluster model including only the first hydration shell in which one water molecule is deprotonated, the calculated absolute pK_a values deviate from the experimental ones with an error as large as 13 pH units for the trivalent cations. The acidity of the metal cations is overestimated, indicating that the deprotonated cluster is calculated to be too stable. Screening the metal cations and the inner sphere by the second hydration shell improves the calculation results substantially, and the deviation decreases to about 6 pH units for the trivalent cations. The result is better for the divalent cations, especially for Fe^{2+}. Overall, the computed data reproduces the observed experimental trend, which shows Mn^{2+} is more basic than Fe^{2+} while Mn^{3+} is more acidic than Fe^{3+} and that the trivalent cations are far more acidic than the divalent cations. Further improvements in the calculations of pK_a values should take into account two important factors we omitted in the theoretical method. The entropy difference term $T\Delta S$ is definitely not negligible and should be included in eq 8 as discussed above. The ionic strength, on the other hand, will shift pK_a values to some extent, especially for the trivalent cations, as cations like Mn^{3+} and Fe^{3+} only exist in strongly acidic solutions and at high ionic strength.[40d] The electrostatic interaction between counterions and solute will stabilize the highly charged systems and balance the overstabilization of the deprotonated clusters, which in turn will raise the absolute pK_a values. Experimentally, pK_a shifts on changing ionic strength have been observed. For example, the experimental pK_a value of Fe^{3+} increases from 2.2 to 2.8 when the ionic strength changes from 0 to 1 M.[44]

5. Roles of Discrete Hydration Shells. The results of the calculations discussed above indicate that the larger cluster model including at least two hydration shells is indispensable in order to compute properties pertaining to solvation phenomena. The role of the first shell is obvious as it is the main cause of the ligand field stabilizing the central metal ions through direct metal−oxygen bonds. The effects of the second shell are not negligible, however, and a more detailed analysis could be instructive.

Table 8 presents the total binding energy difference calculated by subtracting the total binding energy of the small cluster from that of the larger cluster. The solvation energy difference, calculated in a similar fashion, is included as well. If the cluster model is big enough, $\Delta\Delta E_b$ will converge to a value corresponding to product of the number of intershell hydrogen bonds times the strength of each plus a contribution from intrashell hydrogen bonds (in 18-water clusters, there are no intrashell hydrogen bonds, but there will be for larger clusters). Both $\Delta\Delta E_{sol}$ and ΔE_{sol} will eventually decrease to zero, as the solvent will be undisturbed by a very large cluster. ΔE_{sol} is the free energy of solvation of the cluster in the continuum dielectric and, therefore, gives a net lowering of free energy of the cluster in solution compared with the isolated cluster plus bulk solvent. The data in Table 8 indeed show such a trend as the total charge of the clusters is lowered. For the clusters with a net charge of +3, $\Delta\Delta E_b$ is as large as about 270 kcal/mol. This number decreases dramatically to 75 kcal/mol for the +1 cluster, which can be exclusively attributed to the 12 hydrogen bonds between the water molecules in the first and second shells, given the normal hydrogen bond strength of 5−7 kcal/mol.[32] Thus for systems with low charges, a small cluster model might be sufficient to smooth the gap between the first hydration shell and bulk solvent, while for the highly charged systems, larger cluster models with more hydration shells are needed to damp down the perturbation created by the highly charged cations. Such perturbations result in the formation of strong hydrogen bonds between the first and second hydration shells and enhance hydrogen bonding to even further shells. Bergström *et al.*[45] applied an infrared absorption double-difference method to explore the hydration shells of some di- and trivalent metal cations. By isotropic substitution of hydrogen atoms and

Table 8. Binding Energy and Solvation Energy Difference between Large and Small Clusters[a]

M	tot. charge	$\Delta E_b[ML(H_2O)_{12}^{m+}] - \Delta E_b[ML^{m+}]$	$\Delta E_{sol}[ML(H_2O)_{12}^{m+}] - \Delta E_{sol}[ML^{m+}]$
		$ML = M(H_2O)_6$	
Mn^{3+}	+3	272.2	141.7
Fe^{3+}	+3	266.4	137.2
Mn^{2+}	+2	145.2	39.8
Fe^{2+}	+2	146.4	40.1
		$ML = M(OH)(H_2O)_5$	
Mn^{3+}	+2	158.9	34.5
Fe^{3+}	+2	151.6	32.0
Mn^{2+}	+1	74.5	22.8
Fe^{2+}	+1	70.9	27.4

[a] Energies in kcal/mol.

Table 9. Energy Contributions (kcal/mol) to Solvation Energy ΔE_{sol}

	$\Delta E_{sol}^{el}(\rho_g)$	ΔE_{pol}	ΔE_{strain}
$Mn(H_2O)_6^{2+}$	−198.0	−0.1	0.2
$Mn(H_2O)_{18}^{2+}$	−155.0	−8.0	4.9
$Mn(H_2O)_6^{3+}$	−449.0	−1.2	0.4
$Mn(H_2O)_{18}^{3+}$	−306.8	−4.7	3.3
$Fe(H_2O)_6^{2+}$	−198.7	−0.5	0.6
$Fe(H_2O)_{18}^{2+}$	−154.9	−8.4	4.8
$Fe(H_2O)_6^{3+}$	−443.3	−1.1	0.5
$Fe(H_2O)_{18}^{3+}$	−306.1	−5.1	4.4
$Mn(OH)(H_2O)_5^{+}$	−71.5	−10.7	3.8
$Mn(OH)(H_2O)_{17}^{+}$	−89.6	−21.8	10.2
$Mn(OH)(H_2O)_5^{2+}$	−205.6	−2.6	1.5
$Mn(OH)(H_2O)_{17}^{2+}$	−165.1	−12.1	4.8
$Fe(OH)(H_2O)_5^{+}$	−68.9	−9.8	4.5
$Fe(OH)(H_2O)_{17}^{+}$	−96.0	−22.2	16.5
$Fe(OH)(H_2O)_5^{2+}$	−204.8	−3.3	1.4
$Fe(OH)(H_2O)_{17}^{2+}$	−166.8	−11.7	3.8

(45) (a) Bergström, P.-A.; Lindgren, J.; Read, M.; Sandström, M. *J. Phys. Chem.* **1991**, *95*, 7650. (b) Bergström, P.-A.; Lindgren, J. *Inorg. Chem.* **1972**, *31*, 1529.

Table 10. Mulliken and ESP Charges of $M(H_2O)_n^{m+}$

	Mulliken (gas)			ESP(gas)			ESP(solv)		
	M	$6H_2O(1)$	$12H_2O(2)$	M	$6H_2O(1)$	$12H_2O(2)$	M	$6H_2O(1)$	$12H_2O(2)$
$Mn(H_2O)_6^{2+}$	0.932	1.068		1.874	0.126		1.883	0.117	
$Mn(H_2O)_{18}^{2+}$	0.913	0.720	0.367	2.180	0.369	−0.549	2.025	0.489	−0.514
$Mn(H_2O)_6^{3+}$	1.052	1.948		2.149	0.851		2.160	0.840	
$Mn(H_2O)_{18}^{3+}$	0.986	1.363	0.651	2.582	0.737	−0.319	2.379	0.993	−0.372
$Fe(H_2O)_6^{2+}$	0.752	1.248		1.853	0.147		1.868	0.132	
$Fe(H_2O)_{18}^{2+}$	0.874	1.020	0.105	2.250	0.576	−0.826	2.122	0.609	−0.731
$Fe(H_2O)_6^{3+}$	0.961	2.039		2.004	0.996		2.015	0.985	
$Fe(H_2O)_{18}^{3+}$	0.927	1.433	0.640	2.358	0.916	−0.274	2.266	1.083	−0.349

determination of O−H and O−D stretching frequencies, they were able to extract spectra of ion-perturbed HDO molecules and to assign the spectra to the first and second hydration spheres of the cations. They concluded that there is no perturbation of water molecules beyond the primary cation hydration sphere for divalent ions, but the water molecules in the second shell of trivalent cations form hydrogen bonds to further waters that are comparable in strength to those formed by the first-shell water molecules to the second shell in divalent cation complexes.

The calculated solvation energy can be decomposed into several contributions according to[6a]

$$\Delta E_{sol} = \Delta E_{sol}^{el}(\rho_g) + \Delta E_{pol} + \Delta E_{strain} \qquad (10)$$

$\Delta E_{sol}^{el}(\rho_g)$ is the solvation energy from the gas-phase charge distribution in which any solute (discrete cluster) polarization induced by the continuum solvent is neglected. ΔE_{pol} accounts for the solvation energy gained from such solute polarization, while ΔE_{strain} is the electronic energy cost due to charge redistribution or deformation. The calculated values of these terms are presented in Table 9 and show that small clusters, especially $M(H_2O)_6^{m+}$, are very weakly polarizable. The ΔE_{pol} and ΔE_{strain} contributions to solvation energy in such clusters are almost negligible. In general, the ΔE_{pol} and ΔE_{strain} contributions are important in larger clusters and even more important in the metal−hydroxyl systems where there are significant dipole moments.

The highly charged metal center induces a redistribution of the charges over the water molecules in the cluster. The charge of water in the hydration shells may be quite different from that of bulk solvent. Table 10 presents the calculated Mulliken and ESP charges for the clusters in gas phase and in solution. Both the Mulliken and ESP charges show a nonzero total charge for the second shell water molecules, indicating a charge flow or charge transfer between the first and second shells. Dividing the total charge of each shell by the number of water molecules, the net charge carried by each water molecule decreases from the first shell to the second. Compared with the Mulliken charges, the ESP charges on the metal centers are closer to the formal charges and the charge of each of the second shell water molecules is negative although small. Thus the larger cluster with more hydration shells allows charge transfer between the inner and outer shells and modestly increases the charge on the central metal ion based on the ESP charges. These details would be missed in the pure continuum solvent model.

Conclusions

We have demonstrated that the combined density functional and continuum dielectric theory is a useful tool for calculating molecular properties in solution even for highly charged transition metal complexes with net spin. The calculated hydration energies of metal ions and the redox potentials compare fairly well with experimental data. A relatively large deviation still remains for calculated pK_a values of water ligand deprotonation, especially for the systems with higher charge. But the correct trend in the acidity of the metal ions is found, both for the much greater acidity of the M^{3+} compared with $M^{2+}(aq)$ ions and for Mn versus Fe. These calculations pave the road for the future study of active site models of metalloenzymes in which charged and high-spin transition metals are surrounded by low dielectric protein environments.

In addition to devising a suitable theoretical methodology, we have also shown the importance of adopting a reasonable discrete supermolecular cluster model that represents the solute inside the cavity embedded in the dielectric continuum. The calculated redox potentials and pK_a values converge toward experimental data with increasing size of the cluster model. The water molecules in the first hydration shell form direct covalent bonds to the metal center, playing the role of a ligand field to stabilize the ions. The second shell is also indispensable as this buffer shell retains strong hydrogen bonds and electron transfer between the inner and outer shells and offers a better description of the solute−solvent dispersion interaction as well. The higher the charge that the metal center carries, the more shells should be included in the cluster model. Although the necessity of including the second shell in clusters has been discussed,[27e,30d,35,46] this study represents the first test in which the larger cluster model for the hydrated metal cations is considered explicitly with high-level self-consistent field quantum mechanical calculations combined with a continuum dielectric model.

Acknowledgment. This work was supported by NIH Grants GM50154 and GM43278 to L.N. and GM45607 to D.B. We thank E. J. Baerends and the Amsterdam group for the use of ADF and AMOL packages, K. Raymond for suggesting this problem, and C. Y. Peng and D. A. Case for their contributions to the continuum dielectric methodology. The calculations were carried out on the HP 9000/735 workstations at The Scripps Research Institute.

Supporting Information Available: A listing of Cartesian coordinates and ESP charges of all clusters calculated in this paper (11 pages). Ordering information is given on any current masthead page.

IC951428F

(46) Tuñón, I.; Silla, E.; Bertrán, J. *J. Phys. Chem.* **1993**, *97*, 5547.